FRONTIERS OF PHYSICS

RESEARCH ARTICLE
Volume 17 / Issue 4 / 43504 / 2022

Ferroelectricity in hBN intercalated double-layer graphene

Yibo Wang[1,*,†], Siqi Jiang[1,*], Jingkuan Xiao[1], Xiaofan Cai[1], Di Zhang[1], Ping Wang[1], Guodong Ma[1], Yaqing Han[1], Jiabei Huang[1], Kenji Watanabe[2], Takashi Taniguchi[2], Yanfeng Guo[4], Lei Wang[1,3], Alexander S. Mayorov[1,‡], Geliang Yu[1,3,§]

1 National Laboratory of Solid State Microstructures and School of Physics, Nanjing University, Nanjing 210093, China
2 National Institute for Materials Science, 1-1 Namiki, Tsukuba 305-0044, Japan
3 Collaborative Innovation Centre of Advanced Microsctructures, Nanjing University, Nanjing 210093, China
4 School of Physical Science and Technology, Shanghai Tech University, Shanghai 201210, China
Corresponding authors. E-mail: †yibowang@nju.edu.cn, ‡mayorov@nju.edu.cn, §yugeliang@nju.edu.cn
*These authors contributed equally to this work.
Received January 11, 2022; accepted March 11, 2022

ABSTRACT

Van der Waals (vdW) assembly of two-dimensional materials has long been recognized as a powerful tool for creating unique systems with properties that cannot be found in natural compounds [*Nature* 499, 419 (2013)]. However, among the variety of vdW heterostructures and their various properties, only a few have revealed metallic and ferroelectric behaviour signatures [*Sci. Adv.* 5, eaax5080 (2019); *Nature* 560, 336 (2018)]. Here we show ferroelectric semimetal made of double-gated double-layer graphene separated by an atomically thin crystal of hexagonal boron nitride. The structure demonstrates high room temperature mobility of the order of 10 $m^2 \cdot V^{-1} \cdot s^{-1}$ and exhibits ambipolar switching in response to the external electric field. The observed hysteresis is reversible and persists above room temperature. Our fabrication method expands the family of ferroelectric vdW compounds and offers a promising route for developing novel phase-changing devices. A possible microscopic model of ferroelectricity is discussed.

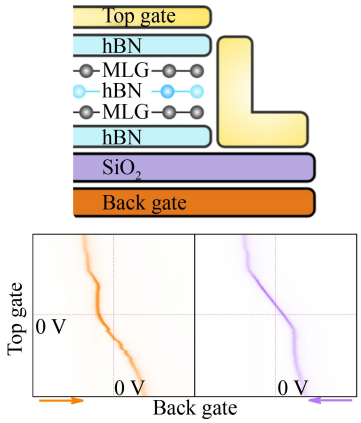

Keywords double-layer graphene, ferroelectric metal, intercalation, dry transfer, high-mobility

1 Introduction

Competing phases in condensed matter demonstrate various physics phenomena: superconductivity and ferromagnetism, charge density wave and superconductivity [4] to name a few. The recently investigated ferroelectric semimetal such as WTe_2 [2, 3] as an example of an unintuitive interplay between polarization and free charge, which seems at first glance, should screen the former. Generally, metallic properties of a material do not favour macroscopic polarization, which means that ferroelectricity as a phenomenon is observed in many ferroelectrics of dielectric nature or semiconducting materials. Only a few examples exist for metallic ferroelectrics and even fewer candidates to show hysteretic

#Special Topic: Two-dimensional Layered Materials and Device Physics (Ed. Lei Wang).

Higher Education Press

arXiv: 2102.12398
https://doi.org/10.1007/s11467-022-1175-0

behaviour [5]. However, there is one experimental evidence of natural 2D ferroelectric semimetal at room temperature: a few-layer WTe_2 [3] made by exfoliation, and another example is artificially made 2D polar metal based on superlattices $BaTiO_3/SrTiO_3/LaTiO_3$ using advantage of molecular beam epitaxy growth [6]. Both of these materials demonstrate a room-temperature ferroelectric effect. A ferroelectric structural transition occurs in bulk (3D) $LiOsO_3$ crystals at 140 K [7]. The interest in these materials has considerably grown due to the possibility of creating new quantum states, including coexisting ferroelectric, ferromagnetic, and superconducting phases [7], use them for functional nanoelectronics applications [2]. It is relevant to the combination of memory effects and conduction modulation, which improves transistor performance [8, 9].

Monolayer graphene (MLG) has high-mobility charge carriers at room temperature with acoustic phonon scattering as a limiting factor [10]. Bilayer graphene (BLG) demonstrates lower mobility at room temperature than MLG, but it is still much larger than any other semiconductors or semimetals known [11–13]. Therefore, it could improve the transport properties of ferroelectric metals based on vdW graphene heterostructures. Previously a breakthrough idea of changing properties of two-dimensional materials by staking them in a different order is useful for constructing the new artificially made vdW heterostructures [1]. For a ferroelectric metal to exist, several criteria need to be suggested: second-order phase transition, breaking inversion symmetry, polarization switchability [5].

Here we explore this general idea to create a recently discovered class of materials that combine semimetallic and ferroelectric properties in a single structure [14]. The effect of the moiré pattern reveals the possibility of forming a strong ferroelectric characteristic for conventional 2D materials such as hexagonal boron nitride (hBN) and BLG [15]. Breaking the inversion symmetry occurs by mechanical stacking of two individual layers under small angle rotation, which opens a new path to create different physical effects in graphene, besides the well-known proximity of graphene to ferromagnets superconductors, 2D materials with spin–orbit interactions. Here we study electronic properties and reproduce the ferroelectric effect in bilayer graphene intercalated with a monolayer hBN up to 325 K and demonstrate a metal-to-insulator transition ferroelectric effect in graphene. We suggest a qualitative model for ferroelectricity based on the stress involved in the structure formed during fabrication.

2 Fabrication

Our device is a multiterminal Hall bar [Fig. 1(a)] made of quasi-twisted bilayer graphene (qTBG) using standard dry transfer technique [16]. Graphene layers in such qTBG are separated by a monolayer of hBN, allowing the graphene layers to be electron transparent. The sandwich is encapsulated between two relatively thick hBN slabs protecting MLG layers from the environment [Fig. 1(b)]. The qTBG heterostructure is connected to metal contacts [10] and endowed with top and bottom gate electrodes allowing independent control over the carrier density in each layer (n_t and n_b, respectively) and relative displacement field between the layers.

3 Results

Using the standard low-frequency lock-in technique, electrical transport measurements are carried out in a ^{3}He variable temperature inset system. Figure 1(d) shows our qTBG sample's resistivity as a function of back-gate voltage, V_{bg}, measured at $T = 2.1$ K and zero top gate voltage, $V_{tg} = 0$ V. It exhibits familiar for high-mobility BLG behaviour with a sharp peak of about

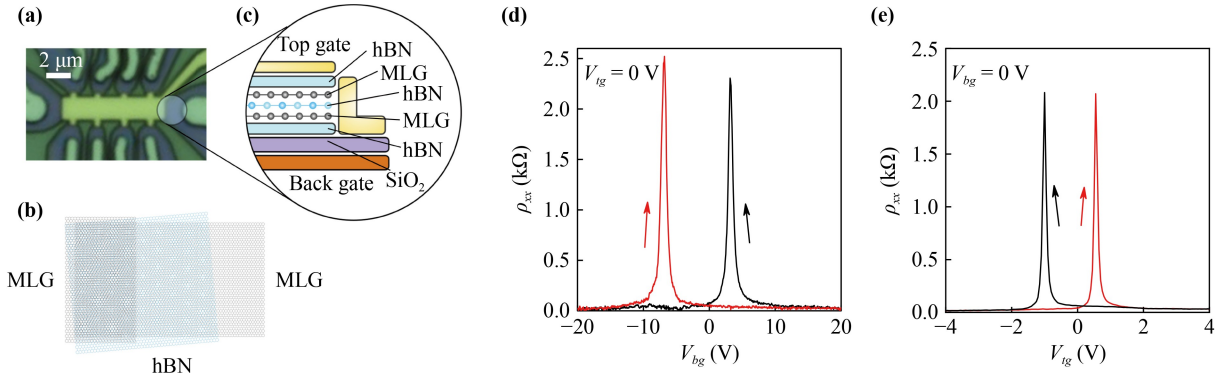

Fig. 1 Hexagonal boron nitride-separated quasi-twisted bilayer graphene. **(a)** Optical photograph of our Hall bar device. An encapsulated qTBG heterostructure is connected to metal leads (dull green) and endowed with gold top gate (bright green) and bottom silicon gate electrodes. **(b)** Schematic of the triple-layer structure. Two MLG layers are twisted by a small twist angle. **(c)** The schematic of the qTBG device with top and bottom gates. **(d, e)** The device's resistivity measured as a function of V_{bg} and V_{tg} at 2.1 K for $V_{tg} = 0$ V and $V_{bg} = 0$ V, respectively.

2 kΩ corresponding to the charge neutrality point (CNP), followed by a rapid decrease with increasing V_{bg}. When the gate voltage's sweep direction is reversed, the resistivity curve is shifted so that the CNP appears at 7 V, more than 10 V away from its initial position. The observed hysteresis is robust and reproduces itself for numerous gate (top and bottom) voltage sweep loops without an apparent sign of degradation of the hysteretic behaviour at low temperature, as shown in supplementary for the case of the resistivity colour map. A similar hysteresis is observed for the top gate sweep measured at $V_{bg} = 0$ V. Notice the CNP position, which is shifted to positive top gate voltages for the forward sweep and negative voltage for the backward sweep.

To confirm the existence of the hysteretic behaviour related to ferroelectricity, we demonstrate the resistance measurements at elevated maximum gate voltage (Fig. 2). Figure 2(a) shows resistance dependence on the back gate voltage measured at 2.1 K for different maximum voltages. At the start, the resistance maximum is observed around zero gate voltage, and the backward and forward sweeps have a small hysteresis. By increasing the maximum gate voltage range, the position of the resistance maximum shifts towards the polarity of the back voltage used without a limit. This effect potentially has two explanations: the presence of the ferroelectric state or the charged traps with slow dynamics. The rule out the trap mechanism, we have measured the presence of spontaneous polarisation, which is clearly seen in Fig. 2(b) for the top gate voltage backwards and forward sweeps. Starting from a small voltage range, the resistance does not cross the resistance maximum, but with increasing the gate voltage range, the resistance peak appears, and it does not change its position significantly for the same polarity of the top gate. It is an indication of the maximum spontaneous polarisation in our structure. The transients characteristics on Fig. 2(c) are revealing a bistable state that is characteristic for regular ferroelectric polarization and demonstration of the possible usage of the device for a transistor with memory. More data on the memory effect are shown in the supplementary.

We review the observed hysteretic behaviour of resistivity of the qTBG intercalated with monolayer hBN in more detail. Previously, a moiré heterostructure hBN/bilayer graphene/hBN has demonstrated a similar hysteresis at low temperatures [15]. The resistivity map is measured as a function of the back gate voltage which charges from −40 V to 40 V for the forward sweep Fig. 3(a) and 40 V to −40 V for the backward sweep [Fig. 3(b)]. Both maps are measured at 2.1 K, and the top gate voltage is fixed during the sweep. The top gate voltage changes from negative to positive values (from −5 V to 4 V). The dark region shows a noticeable difference in the resistivity peak position between the forward and backward sweeps. We plot Fig. 3(c) the maximum resistivity for the forward and backward back gate voltage sweeps to characterize the hysteresis. The hysteretic behaviour illustrates internal polarization in the heterostructure [15], which changes the charge carrier concentration in both graphene layers. The external electric field created by the back and top gate voltages can reverse this polarization by applying a large back gate voltage ($|V_{bg}| > 10$ V) or top gate voltage $V_{tg} < -2.2$ V and $V_{tg} > 1.5$ V. The peak shifts linearly in the range of V_{bg} from −9.1 V to 9.7 V, which corresponds to a linear polarization for ferroelectrics [17]. The top gate's efficiency with respect to the bottom gate cannot be determined from the top and bottom hBN thicknesses (42.6 nm and 111 nm, respectively) using a small dielectric constant for hBN. If the relative dielectric constant for hBN is taken as 5, then the expected efficiency is about 11.6. However, the dashed lines in Fig. 3(c) correspond to the ratio of $V_{bg}/V_{tg} = 7.6 \pm 0.1$. Therefore, the dielectric environment of graphene is significantly distorted by the ferroelectric effect. In the regions without hysteresis, the resistivity peak shift also does not correspond to the gate's efficiency defined as a coefficient of proportionality, α, between the concentration and the gate voltage ($n = \alpha V_g$). The device undergoes ferroelectric-paraelectric phase transition after thermal cycling as shown in Figs. 3(a)−(c) (see supplementary for the details). In the paraelectric phase, the dielectric constant is linear, and the resistivity of the structure depends strongly on the

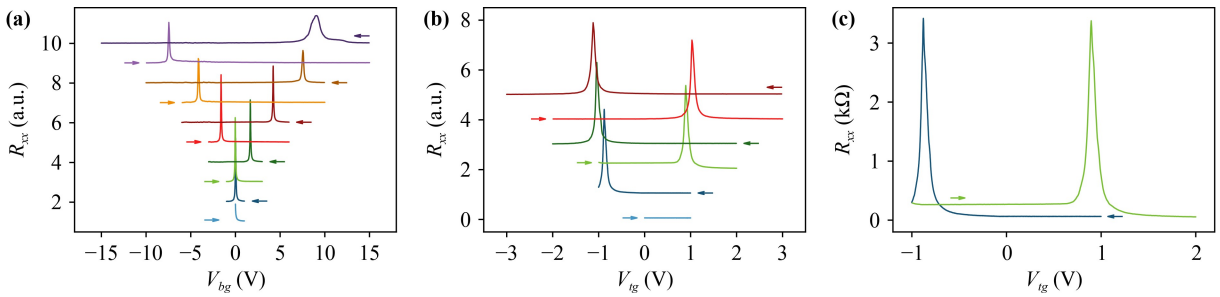

Fig. 2 Gate voltage sweeps with increasing maximum voltage. **(a)** Resistance as a function of V_{bg} for different maximum back gate voltage. The curves are shifted up for clarity. **(b)** Resistance as a function of V_{tg} for different maximum top gate voltage. The curves are shifted up for clarity. **(c)** Two scans from the image (b) shows the memory effect.

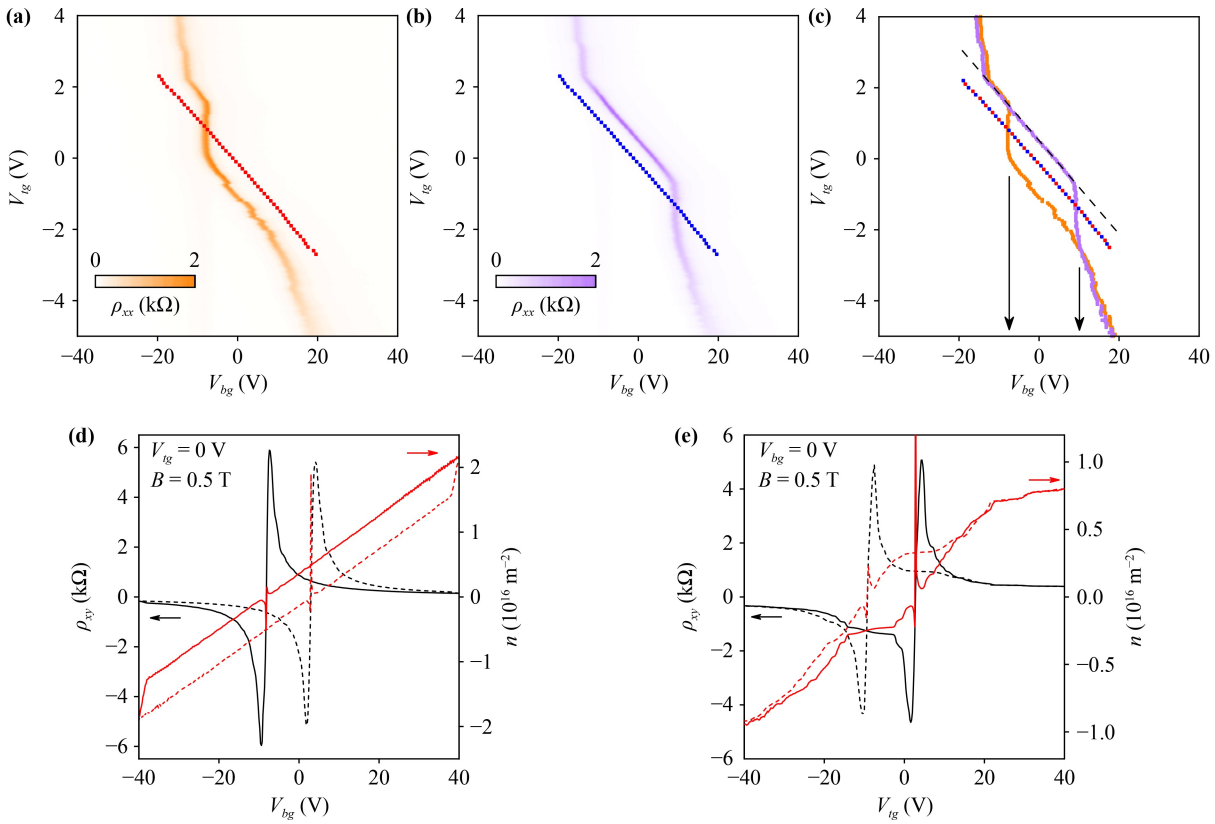

Fig. 3 Ferroelectric hysteresis at 2.1 K. **(a, b)** The sample's resistivity as a function of the back gate and top gate voltages for the forward (a) and backward (b) back gate voltage sweeps at fixed V_{tg}. Scattered data show the position of the maximum resistivity for a paraelectric phase. **(c)** The maximum of the resistivity for the forward and backward as a function of the top gate and back gate voltages. The dashed line is the best fit for the forward and backward sweep's resistivity maxima in the linear ferroelectric regime. The blue and red squares show the maximum resistivity for a paraelectric phase. **(d)** Hall effect measured at $B = 0.5$ T for forward (solid black curve) and backward (dashed black curve) sweeps as a function of back gate voltage at $V_{tg} = 0$ V. The red curves show corresponding concentrations calculated from the Hall voltage. **(e)** Hall effect measured at $B = 0.5$ T for the forward (solid black curve) and backward (dashed black curve) sweeps as a function of top gate voltage at $V_{bg} = 0$ V. The red curves show corresponding concentrations calculated from the Hall voltage.

properties of hBN layers. To the best of our knowledge, this observation has not been reported before in 2D heterostructures.

The average concentration in the system then can be determined by the Hall effect (see supplementary). Calculations of the Hall concentration as a function of back-gate voltage at $V_{tg} = 0$ V are shown in Figs. 3(d) and (e). The resistivity maximum is shifted between the forward and backward shift on the same voltage when the efficiency of the top gate is taken into account. We notice here that the view of this hysteresis and the positions of maxima and minima do not change if top gate voltage sweeps are used at fixed V_{bg} (See supplementary).

Finally, we characterized the temperature dependence of the sample's resistivity for the forward and backward sweeps. The resistivity maximum is reducing with increasing temperature as expected for both MLG and BLG, and the separation between peaks, which is related to spontaneous polarization in our structure, is decreasing with increasing temperature. Still, it does not disappear entirely, even at the maximum available temperature of 325 K [Fig. 4(b)]. The full data set is shown in the supplementary. The cross-over density between metallic ($\mathrm{d}\rho/\mathrm{d}T < 0$) and insulator ($\mathrm{d}\rho/\mathrm{d}T > 0$) states is equal to 5×10^{10} cm^{-2}, which is in agreement with previous report [18]. The corresponding mobility is found to be better than 10 m^2·V^{-1}·s^{-1} at room temperature [Fig. 4(d)], which is higher than in bilayer graphene [19] and comparable with acoustic phonon limited mobility in monolayer graphene [10]. The charge carrier mobility reduces with increasing temperature, as shown in Fig. 4(d) linearly.

4 Discussion

Previously a strong ferroelectric effect was observed in aligned and rotated by 30° hBN/bilayer graphene heterostructures [15]. The authors argued that the different parts of a supercell could induce spontaneous polarization in such a structure. Here we study a similar system without intentional alignment between hBN and

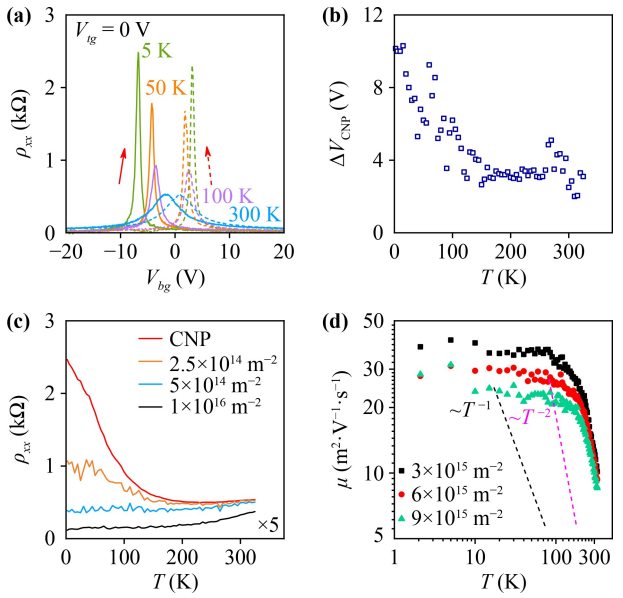

Fig. 4 Transport properties at high temperatures. **(a)** The temperature dependence of the resistivity as a function of back gate voltage at $V_{tg} = 0$ V for the forward (solid style) and backward sweeps (dashed style) for four selected temperatures. **(b)** The voltage difference between CNP positions of the backward and forward sweeps. The temperature changes from 2 K to 325 K. **(c)** The temperature dependence of the resistivity for the forward sweeps for different electron concentrations. The smallest resistivity is multiplied by 5. **(d)** The mobility of electron gas as a function of temperature measured at 3×10^{15} m^{-2}, 6×10^{15} m^{-2} and 9×10^{15} m^{-2}. The dashed lines are guides for the eye.

graphene layers. The angle between the top and bottom MLG is less than 2°. The orientation of the hBN edges and MLG are random. The monolayer hBN edges are not visible in the final stack. The absence of any supercell at low energy could be justified by the gate voltage dependence of the resistance. In this case, the band structure should have more features at low energy, which creates extra CNPs as was reported in Ref. [20]. Also, our device does not show Brown–Zak oscillations [21], which could be an indication of alignment between graphene and hBN. Therefore, our system's ferroelectric effect could not be of the same origin as in the intentionally aligned graphene/hBN structure [15]. However, we could not convincingly exclude 30° rotation [15] or the inversion symmetry breaking in the vertical graphene/hBN/graphene heterostructure as a cause of ferroelectricity. The twisted hBN layers can demonstrate the ferroelectric effect [22]. This observation was reported in Refs. [23, 24]. We can assume that the monolayer hBN can be easily twisted by sliding between two graphene layers. In that case, the polarization can be created by the top hBN and monolayer hBN or between monolayer hBN and bottom hBN layers for the case of 30° rotation [15].

Now we can speculate on the possible origin of the ferroelectric effect. We notice that the structure is made at the 110 ℃, which is a standard temperature for the dry transfer procedure. It is known that the thermal coefficient of expansion for hBN is negative [25]. Therefore, a fast cooldown of the heterostructure made of the monolayer of BN placed between the thick BN layers on SiO_2 substrate (with a positive thermal coefficient of expansion) induces the film's strain. At low temperatures, it expands. Previously, piezoelectric strains have been measured in BN bubbles of monolayer BN [26]. The effect is related to the polar lattice of BN. To form an out-of-plane dipole, the B-sublattice should be shifted up or down with respect to the N-sublattice. This effect will partially negate in-plane strain in the film. The polarization of a single layer of BN should be proportional to the square root of temperature due to geometrical consideration near room temperature as the thermal expansion is a linear function of temperature near room temperature [25]. Asymmetry between the top and bottom gate is possibly caused by different Si and top gate metal thermal expansion. If some N atoms are aligned with B atoms, then a region with no polarisation is formed. This effect reduces the overall polarisation of the structure but increases the strain, which needs further investigation.

Another explanation often used to explain hysteretic behaviour is related to charge traps in the dielectric layer. It is common to deep observer levels in SiO_2 due to defected structure. However, the distance from the conducting layer is too long, and therefore the charging state of these levels does not change with the externally applied voltage. It could be viewed as a small fixed voltage in the capacitance formed by the charged layer and the conducting plate. Therefore the hysteresis could be observed only with respect to thermal cycling when the charging of these traps can be changed. The smaller distance between the traps and the MLG is an essential requirement for the resistance hysteresis as a function of gate voltage. The symmetry between positions of the maxima in forwarding and backward directions could be caused by the symmetric energy distribution of the charged traps close to graphene layers. Potentially the presence of the state without hysteresis after thermal cycling [for example, Fig. 3(a)] could be explained by the strong energy shift of these traps after warming up. That distribution is unlikely as it is not observed in any systems except to a single type of impurity or defect. In that case, the impurity states should be located near the Dirac point in graphene; otherwise, it contradicts the symmetric distribution of the resistance peak position. Due to the strong dependence of the tunnelling on the distance, the space distribution is also delts-like; otherwise, the resistance peak should be broad as it will depend on the exponentially long tunnelling times. Therefore the required distribution of the levels to explain hysteretic behaviour should fulfil two strict criteria: zero energy with respect to the graphene Dirac point and the same position with respect to the

graphene layers. However, the tunnelling probability depends exponentially on the temperature, and the time position of the neutrality points between the forward and backward sweeps should also demonstrate exponential behaviour, which is not observed experimentally (see supplementary). Nevertheless, the observation of the switch of the Hall voltage as shown in Fig. 3(e) could not be explained by any trap distribution. Also, the mobility of our structure is very high, and in the case of closely separated charged traps, the resistance peak should be broadened. We dismissed the trap origin of the observed hysteresis.

Mobility of the charge carriers in MLG at high temperature is limited by acoustic phonon scattering [10]. The temperature dependence of mobility is inversely proportional to temperature. This observation is valid for graphene and its bilayer [27]. The temperature dependence of resistivity is proportional to $\rho \propto T$ in the case of twisted bilayer graphene, which was observed experimentally [28] and predicted theoretically [29] for small angles of rotation. Our observations demonstrate inverse parabolic dependence of the mobility $\mu \propto T^{-2}$ as shown in Fig. 4(d), which does not contradict to the contribution of optical phonons in hBN substrate [30] or polar optical phonons [31]. However, the most probable origin is the effect of Coulomb drag resistance in the double graphene layer structures separated by a thick hBN film (>1 nm) without interlayer tunnelling also demonstrates $\rho \propto T^2$ dependence [32]. The deviation of mobility from this dependence at low temperature is explained by scattering at the edges of the sample.

We have demonstrated ferroelectric−paraelectric transition in metal-like ferroelectric based hBN intercalated double-layer graphene. The high-mobility graphene ferroelectricity survives above room temperature, which shows promising for ferroelectric transistors.

5 Methods

5.1 Transport measurements

The device was measured in an Oxford Instruments TeslatronPT cryogen-free superconducting magnet system equipped with Oxford Instruments HelioxVT Sorption Pumped ^{3}He Refrigerator insert (300 mK, 14 T) and the magnetic field applied perpendicular to the plane of the film. Stanford Research Systems SR830 lock-in is used to apply an AC bias current with a 100 MOhm bias resistor at a frequency of 13.333 Hz, and Keithley 2614B SourceMeters were used to apply DC current with a 100 MOhm bias resistor. Keithley 2400 SourceMeters were used to apply voltages to the gates.

5.2 AFM and Raman measurements

AFM measurements are performed with a Bruker Dimension Fastscan system at tapping mode. Scan area of the bottom/top hBN are shown in the right/left red dotted boxes in the supplementary. The length to width ratio is 1.16. The width of the sample is 2.7 μm. The top and bottom hBN thicknesses are equal to 42.6 nm and 111 nm, respectively.

Room temperature Raman scattering is performed using a WITec/alpha 300R confocal microscope with a 532 nm laser under ambient conditions. The laser power was kept below 1 mW to avoid damage or heating. The G and 2D peaks in the Raman spectra are fitted with Lorentzian. Typical Raman spectra of different positions of the heterostructure are plotted in the Supplementary.

Acknowledgements This work was supported by the National Key R&D Program of China (Grant Nos. SQ2018YFA030066 and SQ2018YFA030143), the National Natural Science Foundation of China (No. 11974169), the Fundamental Research Funds for the Central Universities (Nos. 020414380087 and 020414913201), and the Basic Research Program of Jiangsu Province (Grant No. BK20190283).

Author contributions statement A.S.M. and G.Y. designed the project. Y.W. fabricated the samples, S.J. and J.X. performed transport measurements, X.C. and G.M. did the AFM and Raman research, K. W. and T.T. provided hBN crystals. S. J., J.X., Y.W., and A.S.M performed data analysis, D.Z., P.W., G.M., Y.H, J.H., and A.S.M provided the experimental support. Y.W., A.S.M and G.Y. wrote the manuscript. All authors participated in the discussions.

Competing interests The authors declare no competing interests.

Electronic supplementary materials are available in the online version of this article at https://doi.org/10.1007/s11467-022-1175-0 and https://journal.hep.com.cn/fop/EN/10.1007/s11467-022-1175-0 and are accessible for authorized users.

Correspondence and requests for materials should be addressed to Y.W, A.S.M. or G.Y.

References

1. A. K. Geim and I. V. Grigorieva, Van der Waals heterostructures, *Nature* 499, 419 (2013)
2. P. Sharma, F. X. Xiang, D. F. Shao, D. Zhang, E. Y. Tsymbal, A. R. Hamilton, and J. Seidel, A room-temperature ferroelectric semimetal, *Sci. Adv.* 5, eaax5080 (2019)
3. Z. Fei, W. Zhao, T. A. Palomaki, B. Sun, M. K. Miller, Z. Zhao, J. Yan, X. Xu, and D. H. Cobden, Ferroelectric switching of a two-dimensional metal, *Nature* 560, 336 (2018)
4. X. Xi, L. Zhao, Z. Wang, H. Berger, L. Forró, J. Shan, and K. F. Mak, Strongly enhanced charge-density-wave order in monolayer $NbSe_2$, *Nat. Nanotech.* 10, 765 (2015)
5. W. X. Zhou and A. Ariando, Review on ferroelectric/polar metals, *Jpn. J. Appl. Phys.* 59, SI0802 (2020)

6. Y. Cao, Z. Wang, S. Y. Park, Y. Yuan, X. Liu, S. M. Nikitin, H. Akamatsu, M. Kareev, S. Middey, D. Meyers, P. Thompson, P. J. Ryan, P. Shafer, A. N' Diaye, E. Arenholz, V. Gopalan, Y. Zhu, K. M. Rabe, and J. Chakhalian, Artificial two-dimensional polar metal at room temperature, *Nat. Commun.* 9, 1547 (2018)
7. Y. Shi, Y. Guo, X. Wang, A. J. Princep, D. Khalyavin, P. Manuel, Y. Michiue, A. Sato, K. Tsuda, S. Yu, M. Arai, Y. Shirako, M. Akaogi, N. Wang, K. Yamaura, and A. T. Boothroyd, A ferroelectric-like structural transition in a metal, *Nat. Mater.* 12, 1024 (2013)
8. X. Liu, Y. Yang, T. Hu, G. Zhao, C. Chen, and W. Ren, Vertical ferroelectric switching by in-plane sliding of two-dimensional bilayer WTe_2, *Nanoscale* 11, 18575 (2019)
9. M. Si, A. K. Saha, S. Gao, G. Qiu, J. Qin, Y. Duan, J. Jian, C. Niu, H. Wang, W. Wu, S. K. Gupta, and P. D. Ye, A ferroelectric semiconductor field-effect transistor, *Nat. Nanoelectron.* 2, 580 (2019)
10. L. Wang, I. Mericp, Y. Huang, Q. Gao, Y. Gao, H. Tran, T. Taniguchi, K. Watanabe, L. M. Campos, D. A. Muller, J. Guo, P. Kim, J. Hone, K. L. Shepard, and C. R. Dean, One-dimensional electrical contact to a two-dimensional material, *Science* 342, 614 (2013)
11. C. R. Dean, A. F. Young, I. Meric, C. Lee, L. Wang, S. Sorgenfrei, K. Watanabe, T. Taniguchi, P. Kim, K. L. Shepard, and J. Hone, Boron nitride substrates for high-quality graphene electronics, *Nat. Nanotechnol.* 5, 722 (2010)
12. A. S. Mayorov, R. V. Gorbachev, S. V. Morozov, L. Britnell, R. Jalil, L. A. Ponomarenko, P. Blake, K. S. Novoselov, K. Watanabe, T. Taniguchi, and A. K. Geim, Micrometer-scale ballistic transport in encapsulated graphene at room temperature, *Nano Lett.* 11, 2396 (2011)
13. A. H. Castro Neto, F. Guinea, N. M. R. Peres, K. S. Novoselov, and A. K. Geim, The electronic properties of grapheme, *Rev. Mod. Phys.* 81, 109 (2009)
14. D. Puggioni, G. Giovannetti, M. Capone, and J. M. Rondinelli, Design of a Mott multiferroic from a nonmagnetic polar metal, *Phys. Rev. Lett.* 115, 087202 (2015)
15. Z. Zheng, Q. Ma, Z. Bi, S. de la Barrera, M. H. Liu, N. Mao, Y. Zhang, N. Kiper, K. Watanabe, T. Taniguchi, J. Kong, W. A. Tisdale, R. Ashoori, N. Gedik, L. Fu, S. Y. Xu, and P. Jarillo-Herrero, Unconventional ferroelectricity in moiré heterostructures, *Nature* 588, 71 (2020)
16. A. V. Kretinin, Y. Cao, J. S. Tu, G. L. Yu, R. Jalil, K. S. Novoselov, S. J. Haigh, A. Gholinia, A. Mishchenko, M. Lozada, T. Georgiou, C. R. Woods, F. Withers, P. Blake, G. Eda, A. Wirsig, C. Hucho, K. Watanabe, T. Taniguchi, A. K. Geim, and R. V. Gorbachev, Electronic properties of graphene encapsulated with different two-dimensional atomic crystals, *Nano Lett.* 14, 3270 (2014)
17. M. Lines, Principles and Applications of Ferroelectrics and Related Materials, Clarendon Press, Oxford England, 1977
18. L. A. Ponomarenko, A. K. Geim, A. A. Zhukov, R. Jalil, S. V. Morozov, K. S. Novoselov, I. V. Grigorieva, E. H. Hill, V. V. Cheianov, V. I. Fal'ko, K. Watanabe, T. Taniguchi, and R. V. Gorbachev, Tunable metal–insulator transition in double-layer graphene heterostructures, *Nat. Phys.* 7, 958 (2011)
19. M. Schmitz, S. Engels, L. Banszerus, K. Watanabe, T. Taniguchi, C. Stampfer, and B. Beschoten, High mobility dry-transferred CVD bilayer grapheme, *Appl. Phys. Lett.* 110, 263110 (2017)
20. Z. Wang, Y. B. Wang, J. Yin, E. Tóvári, Y. Yang, L. Lin, M. Holwill, J. Birkbeck, D. J. Perello, S. Xu, J. Zultak, R. V. Gorbachev, A. V. Kretinin, T. Taniguchi, K. Watanabe, S. V. Morozov, M. Anđelković, S. P. Milovanović, L. Covaci, F. M. Peeters, A. Mishchenko, A. K. Geim, K. S. Novoselov, V. I. Fal'Ko, A. Knothe, and C. R. Woods, Composite super-moiré lattices in double-aligned graphene heterostructures, *Sci. Adv.* 5, eaay8897 (2019)
21. R. K. Kumar, X. Chen, G. H. Auton, A. Mishchenko, D. A. Bandurin, S. V. Morozov, Y. Cao, E. Khestanova, M. B. Shalom, A. V. Kretinin, K. S. Novoselov, L. Eaves, I. V. Grigorieva, L. A. Ponomarenko, V. I. Fal'Ko, and A. K. Geim, High-temperature quantum oscillations caused by recurring Bloch states in graphene superlatticess, *Science* 357, 181 (2017)
22. C. R. Woods, P. Ares, H. Nevison-Andrews, M. J. Holwill, R. Fabregas, F. Guinea, A. K. Geim, K. S. Novoselov, N. R. Walet, and L. Fumagalli, Charge-polarized interfacial superlattices in marginally twisted hexagonal boron nitride, *Nat. Commun.* 12, 347 (2021)
23. M. V. Stern, Y. Waschitz, W. Cao, I. Nevo, K. Watanabe, T. Taniguchi, E. Sela, M. Urbakh, and M. B. Shalom, Interfacial ferroelectricity by van der Waals sliding, *Science* 372, 1462 (2021)
24. K. Yasuda, X. Wang, K. Watanabe, T. Taniguchi, and P. Jarillo-Herrero, Stacking-engineered ferroelectricity in bilayer boron nitride, *Science* 372, 1458 (2021)
25. Q. Cai, D. Scullion, W. G. Falin, S. Zhang, K. Watanabe, T. Taniguchi, Y. CHEN, E. J. G. Santos, and L. H. Li, High thermal conductivity of high-quality monolayer boron nitride and its thermal expansion, *Sci. Adv.* 5, eaav0129 (2019)
26. P. Ares, T. Cea, M. Holwill, Y. B. Wang, R. Roldán, F. Guinea, D. V. Andreeva, L. Fumagalli, K. S. Novoselov, and C. R. Woods, Piezoelectricity in monolayer hexagonal boron nitride, *Adv. Mater.* 32, 1905504 (2020)
27. H. Min, E. Hwang, and S. Das Sarma, Chirality-dependent phonon-limited resistivity in multiple layers of graphene, *Phys. Rev. B* 83, 161404 (2011)
28. H. Polshyn, M. Yankowitz, S. Chen, Y. Zhang, K. Watanabe, T. Taniguchi, C. R. Dean, and A. F. Young, Large linear-in-temperature resistivity in twisted bilayer grapheme, *Nat. Phys.* 15, 1011 (2019)
29. F. Wu, E. Hwang, and S. Das Sarma, Phonon-induced giant linear-in-T resistivity in magic angle twisted bilayer graphene: Ordinary strangeness and exotic superconductivity, *Phys. Rev. B* 99, 165112 (2019)
30. I. T. Lin and J. M. Liu, Surface polar optical phonon scattering of carriers in graphene on various substrates, *Appl. Phys. Lett.* 103, 081606 (2013)
31. X. Li, E. A. Barry, J. M. Zavada, M. B. Nardelli, and K. W. Kim, Surface polar phonon dominated electron transport in grapheme, *Appl. Phys. Lett.* 97, 232105 (2010)
32. R. V. Gorbachev, A. K. Geim, M. I. Katsnelson, K. S. Novoselov, T. Tudorovskiy, I. V. Grigorieva, A. H. MacDonald, S. V. Morozov, K. Watanabe, T. Taniguchi, and L. A. Ponomarenko, Strong coulomb drag and broken symmetry in double-layer grapheme, *Nat. Phys.* 8, 896 (2012)